



Thermal stability and pyrolysis characteristics of MTMS aerogels prepared in pure water

Zhi Li · Yan Zhang · Siqi Huang · Xiaoxu Wu · Long Shi · Qiong Liu

Received: 28 May 2020 / Accepted: 21 October 2020 / Published online: 29 October 2020
© Springer Nature B.V. 2020

Abstract Silica aerogel (SA) is a nanoporous material and has attracted increasing attention in the field of thermal insulation in recent years. In this work, the thermal stability and pyrolysis characteristics of the methyltrimethoxysilane (MTMS) silica aerogel (MSA) prepared in pure water were investigated experimentally. The MSA shows a high thermal stability with the onset and peak temperature (T_{onset} and T_{peak}) about 417 °C and 476 °C, respectively, in the pyrolysis process. The oxidation kinetics reveals that the pyrolysis of MSA can be divided into three stages with the average apparent activation energy (E) of each stage being 382.8 kJ/mol, 364.4 kJ/mol, and 328.9 kJ/mol, respectively. The pre-exponential factor (A) has the same tendency with the E . The TG-FTIR analysis demonstrates that the CO₂ and H₂O are the main volatiles during the pyrolysis process and all of them increase against the temperature. It is further observed that the production of CO₂ presents a linear increase, and the H₂O shows an obvious two-stage form along with the temperature. Compared with other hydrophobic SAs,

the MSA has a larger T_{onset} and T_{peak} and much larger E , indicating better thermal safety. The research outcomes provide a technical guide to analyze the thermal pyrolysis of hydrophobic SA and put a new insight to reduce their thermal hazards, which is beneficial to the development of higher-performance nanoporous silica aerogels for the thermal insulation field.

Keywords MTMS aerogels · Thermal stability · Oxidation kinetic · Thermodynamic · Pyrolysis process · Thermal hazard

Introduction

Silica aerogels (SA) as a well-recognized three-dimensional mesoporous (2–50 nm) material usually consist of more than 90% pores and less than 5% solid skeletons (Hüsing and Schubert 1998; Huang et al. 2020), which were initially prepared by Kistler in 1931 (Kistler 1931, 1932). This unique porous structure creates a low density, ultra-low thermal conductivity, and super-high specific surface area (Li et al. 2020), which enable the wide application of SA in thermal insulation areas, such as residential and industrial buildings (Cuce et al. 2014), industrial pipelines (Meador et al. 2009), electronic devices (Zhao et al. 2015), and spacecrafts (Randall et al. 2011). With the development of low-cost preparation technology (Huber et al. 2017; Koebel et al. 2016), the usage of SA in thermal insulation field will continuously increase, while the related research is needed critically to supported the trend.

Z. Li · Y. Zhang · S. Huang · X. Wu · Q. Liu (✉)
School of Resource and Safety Engineering, Central South University, Changsha 410083, People's Republic of China
e-mail: liuqiong@csu.edu.cn

X. Wu
School of Economics and Management, Changsha University, Changsha 410083, People's Republic of China

L. Shi
Civil and Infrastructure Engineering Discipline, School of Engineering, RMIT University, Melbourne, VIC 3000, Australia

As an excellent insulation nanomaterial, its thermal stability and pyrolysis characteristics deeply affect the coverage of the practical applications. Ignoring the thermal hazard would result in low efficiency, failure of thermal insulation, or even bringing fire risk to the public. On this aspect, a lot of studies have been carried out to address the thermal decomposition or degradation of typical polymer insulation materials, e.g., polyurethane (PU) (Jiang et al. 2015), extruded polystyrene (XPS), expanded polystyrene (EPS), etc. However, the flammability and pyrolysis characteristics of pure hydrophobic SA are rarely attracting the public's attention, though our previous studies (Li et al. 2016) have confirmed the significance.

A few studies have been done on the fire safety of aerogel composite materials. In Motahari et al. 2015, Motahari et al. prepared polypropylene (PP)/SA composites and studied their thermal and flammable properties (Motahari et al. 2015). In Martinez et al. 2016, Martinez et al. evaluated the thermal behavior of polyester fiber reinforced SA composites and confirmed their fire classification of B-s1, d0 (Martinez et al. 2016). Other studies also concentrated on the polymer aerogel composites, such as poly(vinyl alcohol)/SA (PVOH/SA) (Chen et al. 2014), and clay aerogels (Finlay et al. 2008; Guo et al. 2013). A more basic problem, namely, the thermal decomposition or degradation of pure SA, should be paid more attention (Wu et al. 2020b), as it plays an important role in determining the thermal hazards before the wide adoption in practice.

Current SAs can be divided into different types due to various silica source and diverse preparation technologies, including solvent, modifiers, modification methods, and drying methods. For the application of thermal insulation, hydrophobic SA is the most frequently used type, which can resist the moisture in air and maintain efficient thermal insulation for a long term. It is widely reported that the hydrophobicity of SA primarily derives from introduced non-hydrolysable organic groups (e.g., alkyl) (He et al. 2019; He and Chen 2017; Li et al. 2019). However, these introduced organic groups not only create the hydrophobicity but also bring a potential thermal hazard, especially when exposed under thermal radiation or fire (Wu et al. 2020a).

In order to eliminating the influence of the irrelevant factors, a simple and easily synthetic hydrophobic SA was chosen for this study. In this study, we firstly prepared methyltrimethoxysilane (MTMS)-based silica aerogels (MSA) in pure water under ambient drying

(APD) and performed the basic characterization. Then we focused on the thermal stability and pyrolysis process of the MSA and tried to clarify their pyrolysis mechanism. Furthermore, the oxidation kinetics was performed using an iso-conversional method to explore the pyrolysis characteristics of MSA. This study shows a good example to further explore the thermal decomposition or degradation of hydrophobic SA aerogels, which is of great importance to their practical thermal insulation applications, and beneficial to the development of SA nanomaterials in thermal insulation field.

Experimental section

Aerogel preparation

Methyltrimethoxysilane (MTMS, Aldrich, 98%) was a precursor and other chemicals including hydrochloric acid (HCl, 36.5%), ammonium hydroxide ($\text{NH}_3 \cdot \text{H}_2\text{O}$, 25.0~28.0%), and cetyltrimethylammonium bromide (CTAB, 99.5%) were chemical pure grade from Sinopharm Chemical Reagent Co., Ltd. (SCRC, China) and used as received.

A typical two-step, acid-base catalyzed sol-gel method was adopted. Firstly, 5-mL MTMS, 30-mL, water and 0.01-g CTAB were mixed in a 100-mL beaker. During the mixing process, 0.3 mL of 0.1 M HCl was added to the mixture, and then the mixture was kept in 45 °C water bath to hydrolyze for 30 min. Subsequently, 0.6 mL of 1 M $\text{NH}_3 \cdot \text{H}_2\text{O}$ was dropped into the mixture to trigger the gelation. Usually the gelation occurs within 1 h at room temperature from the point of $\text{NH}_3 \cdot \text{H}_2\text{O}$ addition. At last, the obtained wet gels were dried under ambient pressure at 60 °C, 80 °C, and 120 °C for 2 h, respectively, to generate MTMS silica aerogels (MSA).

Conventional characterization

The bulk density (ρ_b) of SA was measured by weighing a lump of aerogel of regular geometric shape. The porosity of SA can be then estimated by:

$$\text{Porosity} = \left(1 - \frac{\rho_b}{\rho_s}\right) \times 100\% \quad (1)$$

where ρ_s is the skeleton density of silica, usually 2200 kg/cm³.

A transient hot wire method was used to test the thermal conductivities of the specimens by a thermal constant analyzer (TC3000E XIATECH, China) under 25 °C. Field emission scanning electron microscopy (SEM, SIRION200, FEI) was employed to observe the microstructures of the specimens. A contact angle measurement (CA, SL200K, KINO) was used to characterize the hydrophobicity of the sample by putting 3- μ L water droplets on the sample surface.

Thermogravimetry (TG)

A TA instrument SDT Q600 thermal analyzer was used for thermogravimetry and differential scanning calorimetry (TG-DSC) analysis on SA at the heating rate of 10, 15, and 20 °C/min, respectively. The experiments were conducted at room temperature to 1000 °C in air which was simulated with mixing 80% N₂ and 20% O₂. In the test, the alumina sample crucible was used to load the specimens and three identical samples were tested at each heating rate to ensure the repeatability of the experiments.

Thermogravimetry-infrared spectroscopy (TG-IR)

Fourier transform infrared (FTIR) spectrometer (Nicolet iS50) was employed to characterize the volatiles evolved from the TG furnace under air atmosphere at a heating rate of 10 °C/min. Toward this end, the FTIR and the TG instruments were connected by a transfer line, which was heated and kept at 200 °C to avoid the condensation of the volatiles during the pyrolysis.

Kinetics methods

According to the Arrhenius equation, the relationship between the reaction rate and the reaction temperature can be obtained in a chemical reaction as follows:

$$-\frac{d\alpha}{dt} = Ae^{\frac{-E}{RT}}f(\alpha) \quad (2)$$

where A is the pre-exponential factor; E is the apparent activation energy based on Arrhenius equation; R is the ideal gas constant; T is the reaction temperature; $f(\alpha)$ is a certain function of conversion to reflect the reaction model, and α represents the conversion rate of the reaction, which can be calculated by the ratio of the real-time mass loss to the total mass loss.

As reported extensively, the iso-conversional method is easy to calculate the apparent activation energy without knowing the reaction mechanism. Compared to the single heating rate method (e.g., Coats-Redfern method (Santos et al. 2004; Ebrahimi-Kahrizsangi and Abbasi 2008)), the iso-conversional method is considered to be more reliable. The Flynn-Wall-Ozawa method (FWO) and Kissinger-Akahira-Sunose method (KAS) are the two representative iso-conversional methods (Bigda and Mianowski 2006; Collazzo et al. 2017; Vlaev et al. 2007; Xu and Chen 2013a, 2013b; Ahmad et al. 2017), which have been used widely in the thermal kinetics. In this work, we adopted the FWO and KAS to calculate the apparent activation energy and mutually verified the reliability of the results.

Flynn-Wall-Ozawa method (FWO)

The FWO method is an integral conversional method to get relevant parameters suiting for some integral measurements, e.g., thermogravimetry (TG). For the FWO method, the Doyle's approximation was used to serve the temperature integral (Doyle 1962), and then the FWO method can be described as follow:

$$\ln\beta = \ln\left(\frac{AE}{R}\right) - \ln g(\alpha) - 5.3305 - 1.052 \frac{E}{RT} \quad (3)$$

where β is the heating rate, α is the conversion value, and $g(\alpha)$ is the integral form of the reaction model. The plot of $\ln\beta \sim 1/T$ is a straight line in the series of measurements with various heating rates at the fixed conversion value. The slopes of the fitting lines are employed to calculate apparent activation energy.

Kissinger-Akahira-Sunose method (KAS)

The KAS method is another integral method similar to the FWO method based on the following equation (Wu et al. 2020a, 2020b; Zhang et al. 2019):

$$\ln \frac{\beta}{T^2} = \ln \frac{AR}{Eg(\alpha)} - \frac{E}{RT} \quad (4)$$

After obtaining the curve with $\ln(\beta/T^2)$ and $1/T$, apparent activation energy can be calculated from the slope.

The pre-exponential factor (A) can be calculated as follows (Xu and Chen 2013a, 2013b; Maia and de Moraes 2016; Kim et al. 2010):

$$A = \beta E_{\alpha} \exp\left(\frac{E_{\alpha}}{RT_m}\right) / RT_m^2 \quad (5)$$

in which T_m represents the peak temperature on DTG, which was determined under the commonly used heating rate of 10 °C/min (Wu et al. 2018; Cheng et al. 2017; He et al. 2017; Gurav et al. 2009), unless specified.

Results and discussion

Properties of silica aerogels

Microstructure

Figure 1 is the typical microstructure of the as-prepared MSA, in which the coralloid skeletons with microporous structure in Fig. 1a are similar to that of ref. (Kanamori and Nakanishi 2011). The highly porous and finer structure in Fig. 1b shows that the skeletons look like the branches of corals with slightly crossing and connecting between each other. Actually, the skeletons are still comprised of crosslinked silica nanoparticles ($\ll 100$ nm). Besides, it is hard to find the regular and intact particles in the MSA, which is very different from the MSA prepared in an ethanol/water co-solvent system (Luo et al. 2019). This may be presumed that

they have been replaced by short branches formed by the fusion of several initial particles.

The other relevant parameters are listed in Table 1. The density is as low as 0.077 g/m³ and the porosity is high up to 96.50%. The typical thermal conductivity of the as-prepared MSA in this work is about 0.0395 W m⁻¹ K⁻¹, which is lower than that the reported MSA (Cai and Shan 2015), presenting an obvious advantage in thermal insulation performance. However, compared to the classical TEOS-based aerogels (Li et al. 2018), the MSA still has a larger thermal conductivity. The reason should be ascribed to the micro-skeletons and pores in the MSA, which provide better and more thermal passages for heat. In spite of that, the thermal conductivity of the prepared MSA is still competitive as insulation materials.

FTIR and hydrophobicity

The FTIR spectra of MSA are presented in Fig. 2. It can be seen clearly that the prominent peaks ranging from 1000 to 1150 cm⁻¹ correspond to the symmetric and asymmetric modes of Si–O–Si and the typical Si–OH groups appear around 3400 cm⁻¹ and 1650 cm⁻¹. The marks of successful surface modification are C–H bonds and Si–C bonds which are both derived from non-hydrolysable Si–CH₃ groups. For C–H bonds, the common wavenumber is approximately 2960 cm⁻¹. Both Si–C and C–H bonds constitute the chemical foundations for the hydrophobicity. The contact angle (CA) of MSA is about 136° as shown in Fig. 2b, which indicates a nice hydrophobicity of the MSA.

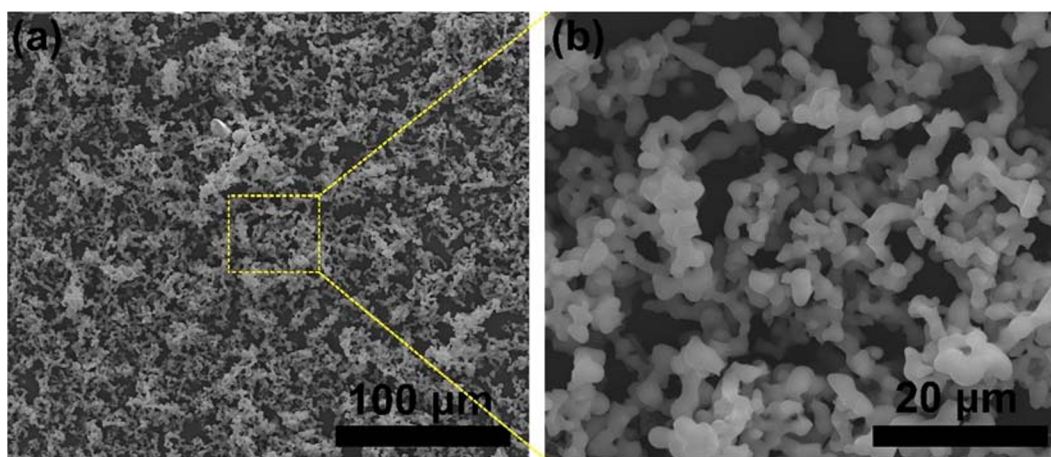


Fig. 1 SEM pictures of the MSA

Table 1 Physicochemical parameters of the MSA

Sample	Density (kg/m ³)	Porosity (%)	Thermal conductivity (W/m/K)
MSA	0.077 ± 0.007	96.50 ± 0.32	0.0395 ± 0.0021

Thermal stability

Figure 3 shows the representative TG-DSC curves for the MSA. From the test start to ~400 °C, a slight weight loss can be observed, which belongs to the evaporation of residuals in the MSA, such as water, unreacted precursor, or their derivatives and the surfactant, CTAB (Luo et al. 2019).

The main weight loss of the MSA occurs during 400~600 °C, corresponding to the thermal oxidation of organic groups, i.e., Si-CH₃ groups on the MSA. At the same time, there exists an evident peak on the DSC curve, indicating the attribution of exothermic reaction for the thermal oxidation of Si-CH₃ groups (He et al. 2019). After 600 °C, the weight of the MSA still decreases gradually till close to 1000 °C. At this stage, the weight loss primarily ascribe to the condensation reaction among the remained and generated Si-OH groups (Zhuravlev 2000; Huang et al. 2017). The mass of the residual is about 85%.

To further address the thermal stability, we have analyzed several special parameters on the TG-DSC curves, namely, the T_{onset} , T_{peak} and T_{end} , which represent the beginning, peak, and end temperatures of a thermal reaction. For hydrophobic SAs, e.g., MSA, when the temperature exceeding the T_{onset} , the hydrophobicity would vanish gradually, transferring to hydrophilia, which results in absorbing water vapor in

air and degenerating properties [22]. The T_{peak} indicates the fastest reaction rate at this specific temperature. Here, the T_{peak} corresponds to the exothermic reaction of the thermal oxidation of Si-CH₃ groups. Table 2 has listed the detailed T_{onset} , T_{peak} , and T_{end} from the DSC curves of the MSA.

It can be seen in Table 2 that the T_{onset} , T_{peak} , and T_{end} all increase with the heating rate. Furthermore, the T_{onset} changes more obviously with the heating rate, when compared to the T_{peak} . It is noted that the average T_{onset} reaches as high as 416.8 °C, which is far higher than that of trimethylsilyl (TMS) modified hydrophobic SAs, with the usual T_{onset} of 240~300 °C (Li et al. 2017). This can demonstrate that compared to the common TMS modified hydrophobic SAs, the MSA possesses higher thermal stability, which gives an advantage for practical thermal protective applications.

Oxidation kinetics and thermodynamics

This section focused on the study of the thermal oxidation kinetics and thermodynamics for the MSA. According to the thermal stability analyses, the T_{onset} and T_{end} of the MSA are 416.8 °C and 593.4 °C, respectively. To concentrate more on the thermal oxidation kinetics of the MSA, a temperature range within 400~600 °C from the TG curves was selected for further analysis as it can avoid the disturbance from unrelated thermal chemical

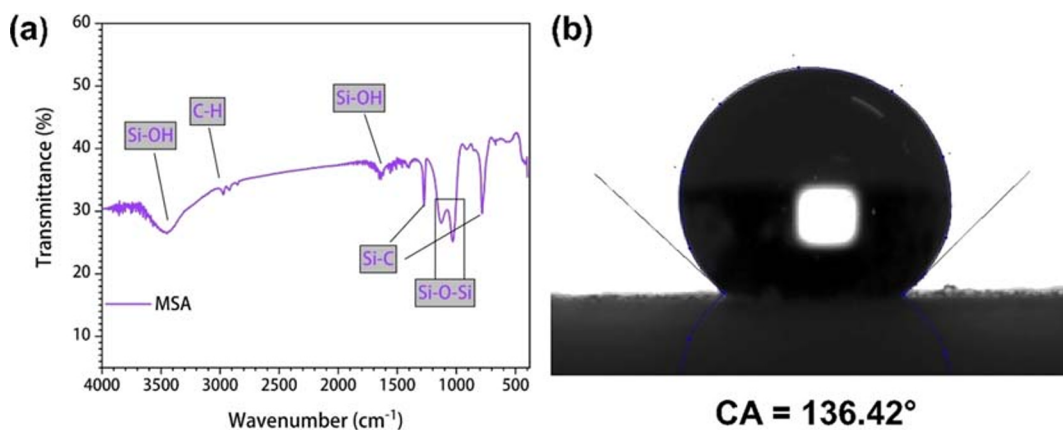
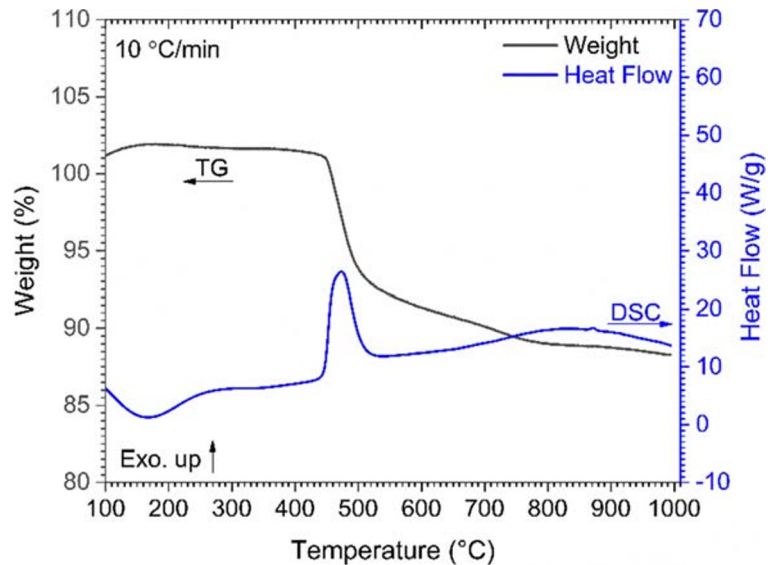
**Fig. 2** a FTIR spectra and b contact angle of the MSA

Fig. 3 Typical TG and DSC curves for the MSA at 10 °C/min in air



reactions. The fitting lines of $\ln(\beta) \sim 1/T$ and $\ln(\beta/T^2) \sim 1/T$ at each conversion rate $\alpha = 0.1 - 0.9$ are presented in Fig. 4. It can be seen that each fitting line at a specific α presents higher linearity, which obeys quite well with Eqs. (3–4).

Figure 5 presents the changes of the E along the conversion rate from 0.1 to 0.8, which can be divided into three stages. Within $\alpha \in (0.7, 0.8)$, the E has an obvious increase. Note that the apparent activation energies calculated when $\alpha > 0.8$ are not reliable. Because some residue which no longer decomposed in the final stage may cause an error in calculating kinetic parameters. As mentioned in the thermal stability section, the weight loss continues till close to 1000 °C. When exceeding a certain temperature ($< T_{end}$), the weight loss becomes complex, which not only includes a small part of the thermal oxidation of Si-CH₃ groups but also contains the condensation reactions of Si-OH groups.

Table 2 The special temperature parameters on DSC curves under various heating rates

Sample	β (°C·min ⁻¹)	T_{onset} (°C)	T_{peak} (°C)	T_{end} * (°C)
MSA	10	406.7	472.1	576.2
	15	419.6	475.5	596.6
	20	424.3	479.2	607.3
	Ave.	416.8	475.6	593.4

*The T_{end} shows a level of variation due to the combination of other thermal chemical reactions at the end of the pyrolysis

Hence, the increasing of the E in this stage actually corresponds to the range of $\alpha \in (0.7, 0.8)$.

At the T_{peak} , the linear fit of $\ln(\beta) \sim 1/T$ and $\ln(\beta/T^2) \sim 1/T$ is shown in Fig. 6, in which the fitting lines of the two methods are almost overlapping. As annotated in Fig. 6, the T_{peak} under the three heating rates ranges in 472.1–479.2 °C, while the corresponding α is within 0.39–0.42. The calculated E based on the FWO and the KAS methods are 427.2 ± 51.0 kJ/mol and 449.4 ± 53.7 kJ/mol, respectively. This is very close to the E at $\alpha = 0.4$, which further indicates that the T_{peak} happens at $\alpha = 0.4$.

When the α increases from 0.4 to 0.7, as shown in Fig. 5, the E decreases obviously, which indicates that certain intermediates during the pyrolysis can facilitate the thermal oxidation of Si-CH₃ groups (Li et al. 2016). Within $\alpha \in (0.1, 0.4)$, the E increases slightly to the highest, about 400 kJ/mol.

In summary, the whole pyrolysis can be divided into three stages, as listed in Table 3. The changes of the apparent activation energy with α present an evidence that the thermal oxidation reaction of the MSA is a multistep process. As we know, the apparent activation energy is the energy which must be provided to trigger a chemical reaction. The larger the apparent activation energy is, the harder the chemical reaction will happen. Therefore, a higher E implies the better thermal stability and thermal safety performance of the MSA.

The \bar{E} expresses the average of the specific stage, which is calculated from apparent activation energies

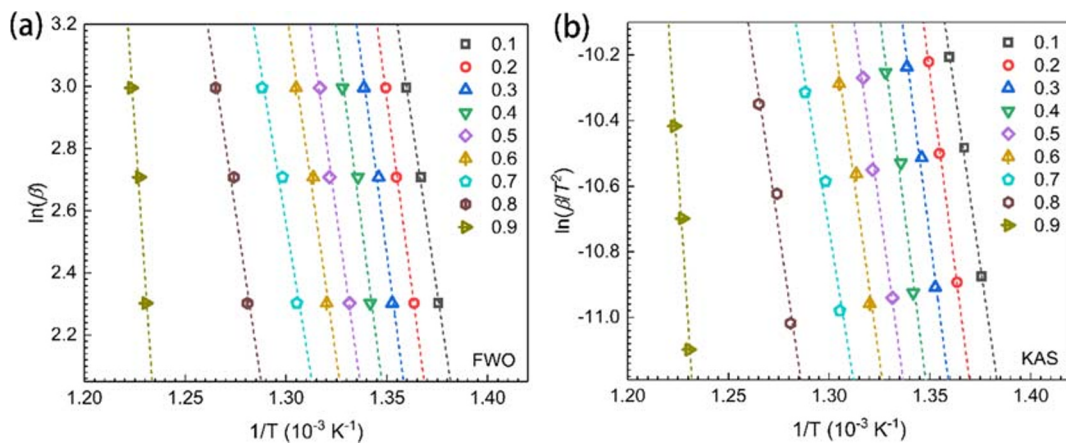


Fig. 4 Fitting lines at various conversion rates based on (a) FWO method and (b) KAS method

(by FWO method) at given α in the corresponding stage.

Furthermore, the pre-exponential factor (A) and the apparent activation energy (E) are illustrated in Fig. 7. The pre-exponential factor (A) is calculated according to Eqs. (5) through the average E obtained from the two methods and the T_m from the TG-DSC curves under 10 °C/min.

Seen from Fig. 7, the change of A keeps the same trend with that of the apparent activation energy (E). Generally speaking, the A reflects the frequency of molecular collisions, which can be directly related to

material structure and reaction types to some extent (Turmanova et al. 2008). In this study, the A ranges from 1.13×10^{20} to 1.35×10^{26} . During Stage I ($\alpha = 0.1 \sim 0.4$), the A increases instantly close to the highest value at $\alpha = 0.4$, indicating a rapidly increasing molecular collision and a sharp need of energy to support the pyrolysis of the MSA (Yuan et al. 2017). In this process, the change of the E also shows a very similar trend. During Stage II ($\alpha = 0.4 \sim 0.7$), the reduced E caused by certain intermediates trigger the thermal oxidation reaction more easily, which also results in a decreasing A . At the

Fig. 5 Variations of the apparent activation energy with different conversion rates, $\alpha = 0.1 - 0.8$

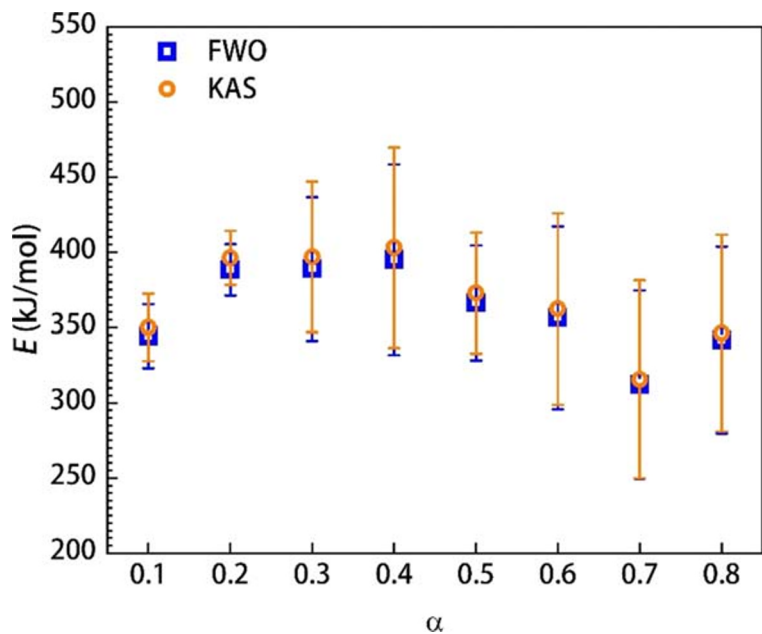
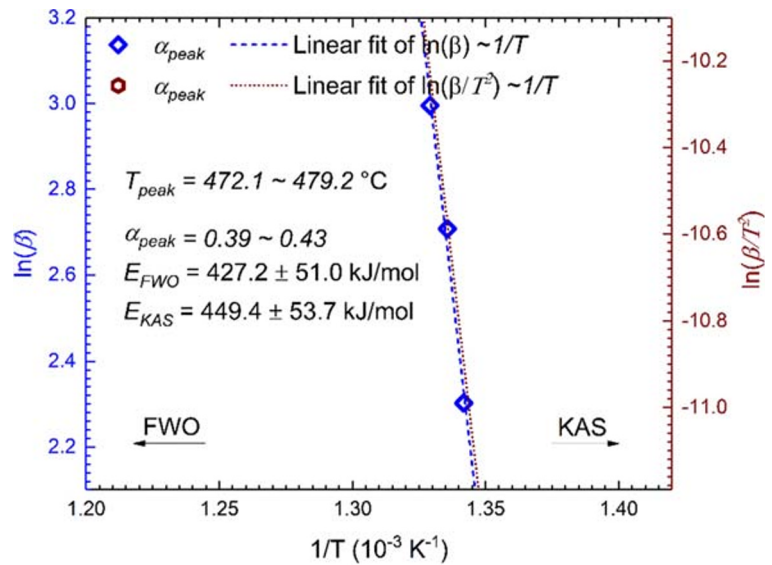


Fig. 6 Fitting lines for the conversion at the T_{peak}



end of the thermal oxidation of Si-CH₃ groups during Stage III ($\alpha = 0.7\text{--}0.8$), other thermal reactions such as the condensation of Si-OH groups could happen. Under this circumstance, the E increases and more energy is then needed to overcome the barrier for these chemical reactions. Meanwhile, the increased A means that the frequency of collisions increases to promote the reaction.

Pyrolysis process

The combination of TG and FTIR (TG-FTIR) can be used to characterize the volatiles in real-time generated during the whole pyrolysis process, which has been presented in a 3D spectrogram shown in Fig. 8. The specific volatile can be confirmed by the characteristic wavenumber or bands and the profile of the given volatile can be acquired by the absorbance against the temperature. It can be seen from Fig. 8

that these volatiles are generated violently after 400 °C, which are quite consistent with the TG-DSC results.

The detailed spectral results are presented in Fig. 9, which takes the volatiles pyrolyzed under 800 °C as an example. The remarkable absorption peaks at 2323 cm⁻¹, 2360 cm⁻¹, and 668 cm⁻¹ correspond to CO₂, which mainly ranges in 2217–2391 cm⁻¹ and 586–726 cm⁻¹ (Liu et al. 2008; Wang et al. 2011; Ding et al. 2016). However, the CO absorption peak located at 2000–2260 cm⁻¹ (Wang et al. 2011) is hard to be observed. The absorption peaks during 3500–4000 cm⁻¹ and 1300–1800 cm⁻¹ are attributed to water (Ding et al. 2016). The pyrolysis of the MSA is a complicated process which is controlled by the combination effects of heat and oxygen. It is speculated that some low molecular weight organics are formed during the pyrolysis process, which are oxidized to water and carbon dioxide finally. The volatiles from the pyrolysis process are summarized and listed in Table 4.

The FTIR spectrums of the volatiles at the specific temperatures from 100 to 800 °C is illustrated in Fig. 10, in which all the spectrums at various temperature show a similar profile, just with some differences on the intensity. It can be seen that the absorbance intensities of all the volatiles, including CO₂ and H₂O, increase with the rising temperature.

More detailedly, the change of CO₂ and H₂O against the temperature is presented in Fig. 11. It is

Table 3 Three stages of the thermal oxidation process

Stage	α	\bar{E} (kJ/mol)
I	(0.1, 0.4)	379.1
II	(0.4, 0.7)	357.5
III	(0.7, 0.8)	326.9

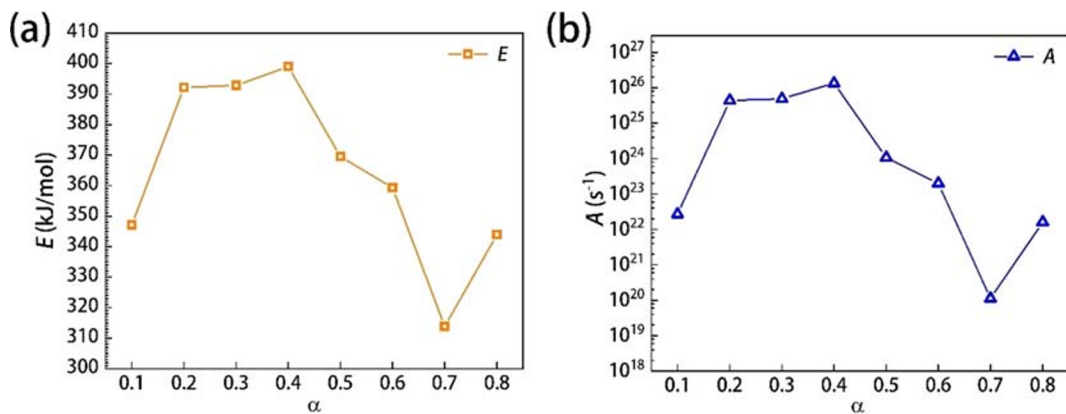
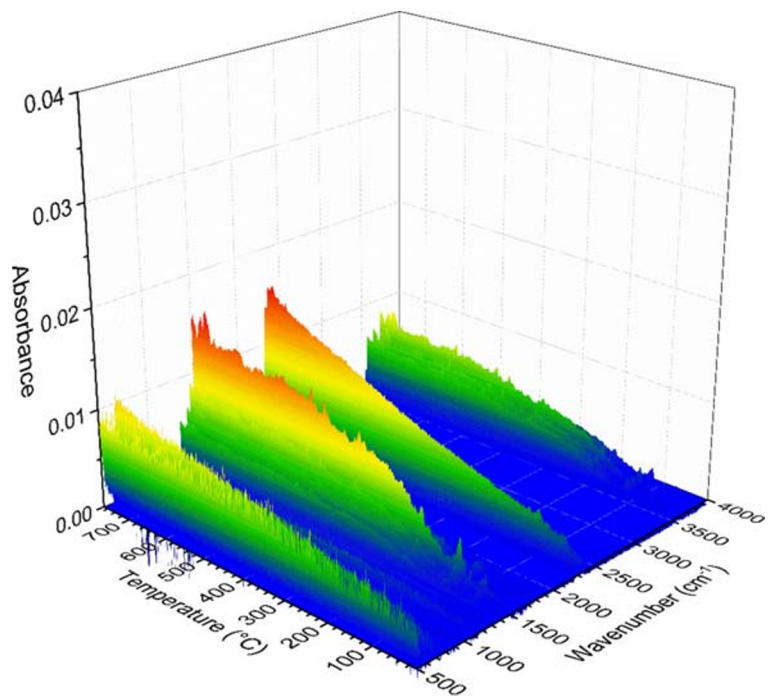


Fig. 7 Thermodynamic parameters for the pyrolysis process of the MSA. **a** apparent activation energy and **b** the pre-exponential factor (A) for the pyrolysis process of the MSA

found that the absorbance of CO_2 linearly increases with the temperature during the whole pyrolysis process as shown in Fig. 11a. The absorbance of the wavenumbers at 2360 cm^{-1} , 2323 cm^{-1} , and 668 cm^{-1} follows the same tendency, which further indicates the formation of CO_2 . In Fig. 11b, the water with the wavenumbers at 3739 cm^{-1} and 1512 cm^{-1} shows a similar variation of the absorbance, which can be divided into two stages with a turning point of about $417\text{ }^\circ\text{C}$ (i.e., T_{onset}). During the Stage I, the

absorbance increases rapidly, which is mainly ascribed to the evaporation of residual water and the pyrolysis products (water). The absorbance at Stage II generally maintains stable, which is derived from the water generated by the condensation between silicon hydroxyl groups (Si-OH). The profiles of CO_2 and H_2O from the pyrolysis process are reported for the first time, which have an important meaning to further understand the preparation and thermal hazard of hydrophobic SAs.

Fig. 8 TG-FTIR spectra of the volatiles during the pyrolysis



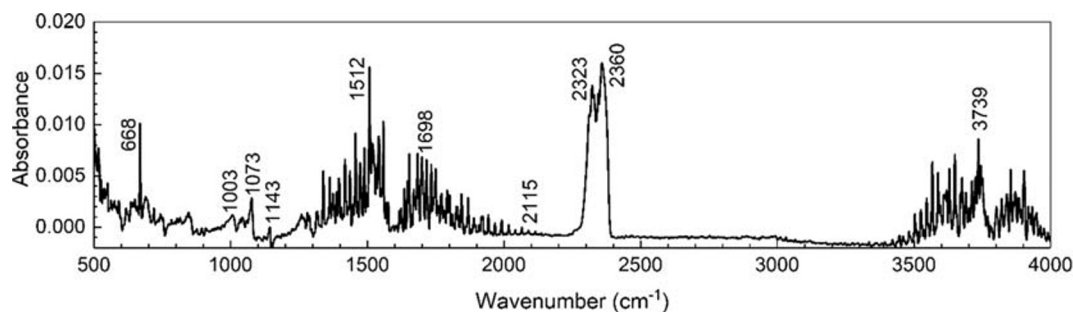


Fig. 9 FTIR of the volatiles at 800 °C

Comparison between the MSA and other hydrophobic SAs

This section focused on the thermal performance comparison between the MSA and other hydrophobic SAs. The related parameters are summarized and listed in Table 5, in which MTSA, DSA, and TSA represent methyltrichlorosilane (MTCS), dimethyldichlorosilane (DMDCS), and trimethylchlorosilane (TMCS) modified hydrophobic SAs, respectively.

It can be seen that the density of the MSA is obviously lower than those of the MTSA, DSA and TSA. The MSA still can satisfy most of the practical applications, though the thermal conductivity is slightly higher than the others. Besides, it is easy to prepare the monolithic MSA via ambient pressure drying (Luo et al. 2019), while the same technology usually results in cracking into granules for the MTSA, DSA, and TSA (He et al. 2015). This feature can further expand the practical applications of the MSA. The outstanding characteristics of the MSA belong to their higher thermal stability and better thermal safety, which can be supported by the far larger T_{onset} , T_{peak} , and E

when compared to those of the MTCSA, DSA, and TSA. Based on these results, it is indicated that the thermal hazard of the MSA is much less than the other typical hydrophobic SAs, which is of great benefit to the practical thermal insulation applications.

Conclusions

The methyltrimethoxysilane (MTMS) based silica aerogels (MSA) showed a low density (0.077 g/cm^3) and thermal conductivity (0.0395 W/m/K), which presented a huge application prospect in the thermal insulation field. In this study, the thermal stability and pyrolysis characteristics of the MSA were investigated experimentally.

The onset (T_{onset}) and peak (T_{peak}) of the MSA were about 417 °C and 476 °C , respectively, which indicated high thermal stability. The oxidation kinetics demonstrated that the pyrolysis process could be divided into three stages with the average apparent activation energy (E) of 382.8 kJ/mol , 364.4 kJ/mol , and 328.9 kJ/mol , respectively. It was revealed that the pre-exponential factor (A) showed a similar tendency with the E . The CO_2 and H_2O were confirmed as the main volatiles from the pyrolysis by TG-FTIR analysis. And these two volatiles increased against the temperature during the whole pyrolysis process. It was observed, for the first time, that the production of CO_2 showed a linear relationship, and the H_2O presented an obvious two-stage form along with the temperature. Compared to other hydrophobic SAs, the MSA manifested a less thermal hazard with higher thermal stability and better

Table 4 A summary of volatiles and functional groups during the pyrolysis

Volatiles/functional groups	Wavenumber range (cm^{-1})
H_2O	1300–1800, 3500–3964
CO_2	586–726, 2217–2391
CO	2000–2260
Hydroxyl group (–OH)	1300–1400

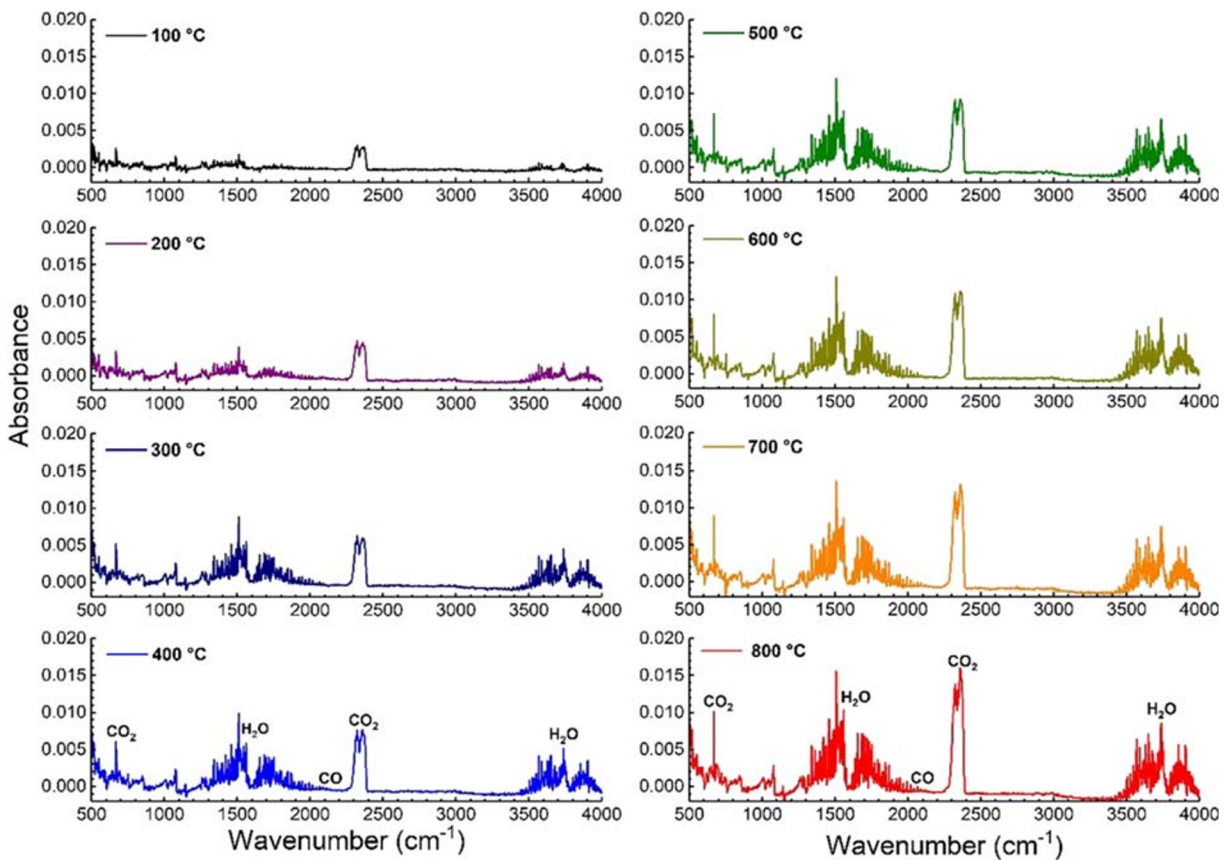


Fig. 10 FTIR of the volatiles during the pyrolysis at specific temperatures

thermal safety, which were vital to the practical thermal insulation applications. The research outcomes provide a technical guide to analyze the thermal pyrolysis of the MSA and put a new

insight to reduce the thermal hazard of hydrophobic SA, which benefits to the expansion of SA materials in the thermal insulation field.

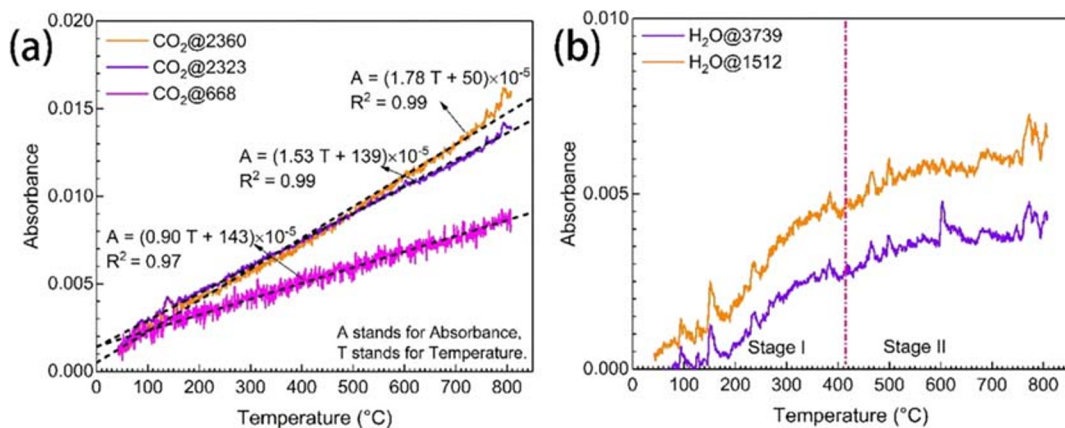


Fig. 11 The profiles of CO₂, H₂O against the temperature

Table 5 The thermal performance of typical hydrophobic SAs

Properties	MSA	MTSA (Zhang et al. 2019)	DSA (Y. Wang et al. 2020)	TSA (Li et al. 2016)
Density (g/cm ³)	0.077	0.130	0.102	0.110
Thermal conductivity (W/m/K)	0.040	0.028	0.028	0.027
Thermal Stability ^a	T_{onset} (°C)	407	242	238
	T_{peak} (°C)	472	277	265
E (kJ/mol) ^b	(314, 399)	(73, 142)	(96, 257)	(58, 184)

^aThe thermal stability is determined by TG-DSC under 10 °C/min

^bFor eliminating the calculation error, the α is set within 0.1–0.8

Funding The authors deeply appreciate the supports from the National Natural Science Foundation of China (No. 51904336), the Natural Science Foundation of Hunan Province (No. 2020JJ4714), the Fundamental Research Funds for the Central Universities (No. 202501003 and 202045001), the Innovation-Driven Project of Central South University (No. 2018CX025), and the Independent Exploration and Innovation Project for Graduate Students of Central South University (2020zzts704).

Compliance with ethical standards

Conflict of interest The authors declare that they have no conflict of interest.

Data availability The raw/processed data required to reproduce these findings cannot be shared at this time as the data also forms part of an ongoing study.

References

- Ahmad MS, Mehmood MA, Taqvi STH, Elkamel A, Liu C-G, Xu J, Rahimuddin SA, Gull M (2017) Pyrolysis, kinetics analysis, thermodynamics parameters and reaction mechanism of *Typha latifolia* to evaluate its bioenergy potential. *Bioresour Technol* 245(December):491–501. <https://doi.org/10.1016/j.biortech.2017.08.162>
- Bigda R, Mianowski A (2006) Influence of heating rate on kinetic quantities of solid phase thermal decomposition. *J Therm Anal Calorim* 84(2):453–465. <https://doi.org/10.1007/s10973-005-7378-0>
- Cai L, Shan G (2015) Elastic silica aerogel using methyltrimethoxysilane precursor via ambient pressure drying. *J Porous Mater* 22:1455–1463. <https://doi.org/10.1007/s10934-015-0026-6>
- Chen HB, Wang YZ, Schiraldi DA (2014) Preparation and flammability of poly(vinyl alcohol) composite aerogels. *ACS Appl Mater Interfaces* 6(9):6790–6796. <https://doi.org/10.1021/am500583x>
- Cheng X, Li C, Shi X, Li Z, Gong L, Zhang H (2017) Rapid synthesis of ambient pressure dried monolithic silica aerogels

using water as the only solvent. *Mater Lett* 204(October): 157–160. <https://doi.org/10.1016/j.matlet.2017.05.107>

- Collazzo GC, Broetto CC, Perondi D, Junges J, Dettmer A, Domelles Filho AA, Foletto EL, Godinho M (2017) A detailed non-isothermal kinetic study of elephant grass pyrolysis from different models. *Appl Therm Eng* 110(January): 1200–1211. <https://doi.org/10.1016/j.applthermaleng.2016.09.012>
- Cuce E, Cuce PM, Wood CJ, Riffat SB (2014) Toward aerogel based thermal superinsulation in buildings: a comprehensive review. *Renew Sust Energ Rev* 34:273–299. <https://doi.org/10.1016/j.rser.2014.03.017>
- Ding Y, Ezekoye OA, Lu S, Wang C (2016) Thermal degradation of beech wood with thermogravimetry/Fourier transform infrared analysis. *Energy Convers Manag* 120(July):370–377. <https://doi.org/10.1016/j.enconman.2016.05.007>
- Doyle CD (1962) Estimating isothermal life from thermogravimetric data. *J Appl Polym Sci* 6(24):639–642. <https://doi.org/10.1002/app.1962.070062406>
- Ebrahimi-Kahrizsangi R, Abbasi MH (2008) Evaluation of reliability of Coats-Redfern method for kinetic analysis of non-isothermal TGA. *Trans Nonferrous Metals Soc China* 18(1): 217–221. [https://doi.org/10.1016/S1003-6326\(08\)60039-4](https://doi.org/10.1016/S1003-6326(08)60039-4)
- Finlay K, Gawryla MD, Schiraldi DA (2008) Biologically based fiber-reinforced/clay aerogel composites. *Ind Eng Chem Res* 47(3):615–619. <https://doi.org/10.1021/ie0705406>
- Guo J, Nguyen BN, Li L, Meador MAB, Scheiman DA, Cakmak M (2013) Clay reinforced polyimide/silica hybrid aerogel. *J Mater Chem A* 1:7211. <https://doi.org/10.1039/c3ta00439b>
- Gurav JL, Venkateswara Rao A, Parvathy Rao A, Nadargi DY, Bhagat SD (2009) Physical properties of sodium silicate based silica aerogels prepared by single step sol–gel process dried at ambient pressure. *J Alloys Compd* 476(1):397–402. <https://doi.org/10.1016/j.jallcom.2008.09.029>
- He S, Chen X (2017) Flexible silica aerogel based on methyltrimethoxysilane with improved mechanical property. *J Non-Cryst Solids* 463(May):6–11. <https://doi.org/10.1016/j.jnoncrysol.2017.02.014>
- He S, Li Z, Shi X, Yang H, Gong L, Cheng X (2015) Rapid synthesis of sodium silicate based hydrophobic silica aerogel granules with large surface area. *Adv Powder Technol* 26(2): 537–541. <https://doi.org/10.1016/j.appt.2015.01.002>
- He S, Sun G, Cheng X, Dai H, Chen X (2017) Nanoporous SiO₂ grafted aramid fibers with low thermal conductivity. *Compos*

- Sci Technol 146(July):91–98. <https://doi.org/10.1016/j.compscitech.2017.04.021>
- He S, Huang Y, Chen G, Feng M, Dai H, Yuan B, Chen X (2019) Effect of heat treatment on hydrophobic silica aerogel. *J Hazard Mater* 362(January):294–302. <https://doi.org/10.1016/j.jhazmat.2018.08.087>
- Huang D, Guo C, Zhang M, Shi L (2017) Characteristics of nanoporous silica aerogel under high temperature from 950°C to 1200°C. *Mater Des* 129(September):82–90. <https://doi.org/10.1016/j.matdes.2017.05.024>
- Huang S, Wu X, Li Z, Shi L, Zhang Y, Liu Q (2020) Rapid synthesis and characterization of monolithic ambient pressure dried MTMS aerogels in pure water. *J Porous Mater* 27(4):1241–1251. <https://doi.org/10.1007/s10934-020-00902-3>
- Huber L, Zhao S, Malfait WJ, Vares S, Koebel MM (2017) Fast and minimal-solvent production of superinsulating silica aerogel granulate. *Angewandte Chemie - International Edition* 56(17):4753–4756. <https://doi.org/10.1002/anie.201700836>
- Hüsing N, Schubert U (1998) Aerogels—airy materials: chemistry, structure, and properties. *Angew Chem Int Ed* 37(1–2): 22–45. [https://doi.org/10.1002/\(SICI\)1521-3773\(19980202\)37:1/2<22::AID-ANIE22>3.0.CO;2-I](https://doi.org/10.1002/(SICI)1521-3773(19980202)37:1/2<22::AID-ANIE22>3.0.CO;2-I)
- Jiang L, Xiao H-H, He J-J, Sun Q, Liang G, Sun J-H (2015) Application of genetic algorithm to pyrolysis of typical polymers. *Fuel Process Technol* 138:48–55. <https://doi.org/10.1016/j.fuproc.2015.05.001>
- Kanamori K, Nakanishi K (2011) Controlled pore formation in organotrialkoxysilane-derived hybrids: from aerogels to hierarchically porous monoliths. *Chem Soc Rev* 40(2):754–770. <https://doi.org/10.1039/c0cs00068j>
- Kim YS, Kim YS, Kim SH (2010) Investigation of thermodynamic parameters in the thermal decomposition of plastic waste—waste lube oil compounds. *Environmental Science & Technology* 44(13):5313–5317. <https://doi.org/10.1021/es101163e>
- Kistler SS (1931) Coherent expanded aerogels and jellies. *Nature* 127(3211):741. <https://doi.org/10.1038/127741a0>
- Kistler SS (1932) Coherent expanded-aerogels. *J Phys Chem* 1(36):52–64
- Koebel MM, Huber L, Zhao S, Malfait WJ (2016) Breakthroughs in cost-effective, scalable production of superinsulating, ambient-dried silica aerogel and silica-biopolymer hybrid aerogels: from laboratory to pilot scale. *J Sol-Gel Sci Technol* 79(2):308–318. <https://doi.org/10.1007/s10971-016-4012-5>
- Li Z, Cheng X, Shi L, He S, Gong L, Li C, Zhang H (2016) Flammability and oxidation kinetics of hydrophobic silica aerogels. *J Hazard Mater* 320(December):350–358. <https://doi.org/10.1016/j.jhazmat.2016.07.054>
- Li C, Cheng X, Li Z, Pan Y, Huang Y, Gong L (2017) Mechanical, thermal and flammability properties of glass fiber film/silica aerogel composites. *J Non-Cryst Solids* 457(February):52–59. <https://doi.org/10.1016/j.jnoncrsol.2016.11.017>
- Li Z, Cheng X, Gong L, Liu Q, Li S (2018) Enhanced flame retardancy of hydrophobic silica aerogels by using sodium silicate as precursor and phosphoric acid as catalyst. *J Non-Cryst Solids* 481(August 2017):267–275. <https://doi.org/10.1016/j.jnoncrsol.2017.10.053>
- Li Z, Huang S, Shi L, Li Z, Liu Q, Li M (2019) Reducing the flammability of hydrophobic silica aerogels by doping with hydroxides. *J Hazard Mater* 373(July):536–546. <https://doi.org/10.1016/j.jhazmat.2019.03.112>
- Li Z, Zhao S, Koebel MM, Malfait WJ (2020) Silica aerogels with tailored chemical functionality. *Materials & Design* 193: 108833. <https://doi.org/10.1016/j.matdes.2020.108833>
- Liu Q, Wang S, Zheng Y, Luo Z, Cen K (2008) Mechanism study of wood lignin pyrolysis by using TG–FTIR analysis. *J Anal Appl Pyrolysis* 82(1):170–177. <https://doi.org/10.1016/j.jaap.2008.03.007>
- Luo Y, Li Z, Zhang W, Yan H, Wang Y, Li M, Liu Q (2019) Rapid synthesis and characterization of ambient pressure dried monolithic silica aerogels in ethanol/water co-solvent system. *J Non-Cryst Solids* 503–504(January):214–223. <https://doi.org/10.1016/j.jnoncrsol.2018.09.049>
- Maia AAD, de Moraes LC (2016) Kinetic parameters of red pepper waste as biomass to solid biofuel. *Bioresour Technol* 204(March):157–163. <https://doi.org/10.1016/j.biortech.2015.12.055>
- Martinez G, Roberto EG, Reichenauer G, Zhao S, Koebel M, Barrio A (2016) Thermal assessment of ambient pressure dried silica aerogel composite boards at laboratory and field scale. *Energy and Buildings* 128:111–118. <https://doi.org/10.1016/j.enbuild.2016.06.071>
- Meador MAB, Weber AS, Hindi A, Naumenko M, McCorkle L, Quade D, Vivod SL, Gould GL, White S, Deshpande K (2009) Structure–{property} {relationships} in {porous} 3D {nanostructures}: {epoxy}-{cross}-{linked} {silica} {aerogels} {produced} {using} {ethanol} as the {solvent}. *ACS Appl Mater Interfaces* 1(4):894–906. <https://doi.org/10.1021/am900014z>
- Motahari S, Motlagh GH, Moharramzadeh A (2015) Thermal and flammability properties of polypropylene/silica aerogel composites. *Journal of Macromolecular Science, Part B* 54(9): 1081–1091. <https://doi.org/10.1080/00222348.2015.1078619>
- Randall JP, Meador MA, Jana SC (2011) Tailoring mechanical properties of aerogels for aerospace applications. *ACS Appl Mater Interfaces* 3(3):613–626. <https://doi.org/10.1021/am200007n>
- Santos JCO, Santos IMG, Conceição MM, Porto SL, Trindade MFS, Souza AG, Prasad S, Fernandes VJ, Araújo AS (2004) Thermoanalytical, kinetic and rheological parameters of commercial edible vegetable oils. *J Therm Anal Calorim* 75(2):419–428. <https://doi.org/10.1023/B:JTAN.0000027128.62480.db>
- Turmanova S, Ch S, Genieva D, Dimitrova AS, Vlaev LT (2008) Non-isothermal degradation kinetics of filled with rice husk ash Polypropylene composites. *Express Polym Lett* 2(2): 133–146. <https://doi.org/10.3144/expresspolymlett.2008.18>
- Vlaev LT, Georgieva VG, Genieva SD (2007) Products and kinetics of non-isothermal decomposition of vanadium(IV) oxide compounds. *J Therm Anal Calorim* 88(3):805–812. <https://doi.org/10.1007/s10973-005-7149-y>
- Wang S, Guo X, Wang K, Luo Z (2011) Influence of the interaction of components on the pyrolysis behavior of biomass. *J Anal Appl Pyrolysis* 91(1):183–189. <https://doi.org/10.1016/j.jaap.2011.02.006>
- Wang Y, Li Z, Huber L, Wu X, Huang S, Zhang Y, Huang R, Liu Q (2020) Reducing the thermal hazard of hydrophobic silica

- aerogels by using dimethyldichlorosilane as modifier. *J Sol-Gel Sci Technol* 93(1):111–122. <https://doi.org/10.1007/s10971-019-05170-5>
- Wu X, Fan M, Shen X, Cui S, Tan G (2018) Silica aerogels formed from soluble silicates and methyl trimethoxysilane (MTMS) using CO₂ gas as a gelation agent. *Ceram Int* 44(1):821–829. <https://doi.org/10.1016/j.ceramint.2017.10.005>
- Wu X, Huang S, Zhang Y, Shi L, Luo Y, Deng X, Liu Q, Li Z (2020a) Flame retardant polyurethane sponge/MTMS aerogel composites with improved mechanical properties under ambient pressure drying. *J Nanopart Res* 22(8):221. <https://doi.org/10.1007/s11051-020-04958-9>
- Wu X, Li Z, Joao G, Zhang Y, Huang S, Liu Q (2020b) Reducing the flammability of hydrophobic silica aerogels by tailored heat treatment. *J Nanopart Res* 22(4):83. <https://doi.org/10.1007/s11051-020-04822-w>
- Xu Y, Chen B (2013a) Investigation of thermodynamic parameters in the pyrolysis conversion of biomass and manure to biochars using thermogravimetric analysis. *Bioresour Technol* 146(10):485–493. <https://doi.org/10.1016/j.biortech.2013.07.086>
- Xu Y, Chen B (2013b) Investigation of thermodynamic parameters in the pyrolysis conversion of biomass and manure to biochars using thermogravimetric analysis. *Bioresour Technol* 146(October):485–493. <https://doi.org/10.1016/j.biortech.2013.07.086>
- Yuan X, He T, Cao H, Yuan Q (2017) Cattle manure pyrolysis process: kinetic and thermodynamic analysis with isoconversional methods. *Renew Energy* 107(July):489–496. <https://doi.org/10.1016/j.renene.2017.02.026>
- Zhang W, Li Z, Shi L, Li Z, Luo Y, Liu Q, Huang R (2019) Methyltrichlorosilane modified hydrophobic silica aerogels and their kinetic and thermodynamic behaviors: graphical abstract. *J Sol-Gel Sci Technol* 89(2):448–457. <https://doi.org/10.1007/s10971-018-4882-9>
- Zhao S, Jiang B, Maeder T, Murali P, Kim N, Matam SK, Jeong E, Han YL, Koebel MM (2015) Dimensional and structural control of silica aerogel membranes for miniaturized motionless gas pumps. *ACS Appl Mater Interfaces* 7(33):18803–18814. <https://doi.org/10.1021/acsami.5b05462>
- Zhuravlev LT (2000) The surface chemistry of amorphous silica. *Zhuravlev Model. Colloids Surf A Physicochem Eng Asp* 173(1):1–38. [https://doi.org/10.1016/S0927-7757\(00\)00556-2](https://doi.org/10.1016/S0927-7757(00)00556-2)

Publisher's note Springer Nature remains neutral with regard to jurisdictional claims in published maps and institutional affiliations.